VORTEX GENERATION BEHIND THE CYLINDER CASCADE OF A FAN GRILL

Matej MILAVEC[1], Vlado SCHWEIGER[1], Marko HOČEVAR[2], Matjaž EBERLINC[2], Branko ŠIROK[2]

[1] *Hidria Institut Klima, Aero-acoustic Department, 150 Godovič, 5275 Godovič, Slovenia*

[2] *Faculty of Mechanical Engineering, University of Ljubljana, Aškerčeva c. 6, 1000 Ljubljana, Slovenia*

SUMMARY

The fan guard grill is one of the most important components that contribute to the increased sound power level and dissipation of fluid kinetic energy. Sound power measurements of axial fan operation with and without a guard grill have shown variations in frequency spectra between 800 Hz and 2000 Hz, presumably caused by Karman vortex generation. To analyse Karman vortex generation, air flow around a cascade of cylinder was investigated. The experimental methods included visualisation with oil vapour and measurements of sound power levels in the far field. In addition, numerical LES simulation of air flow around cylinders was performed. Analysis focused on Karman frequency peaks behind cascade of cylinders, -5/3 dissipation law of fully developed isotropic turbulence and sound pressure level of near sound field.

NOMENCLATURE

A - arbitrary observed variable,

B&W – black and white,

D - diameter of cylinder, distance,

f - frequency of velocity fluctuation,

FFT - Fast Fourier Transform,

l_{cil} - length of cylinder,

LES - Large Eddy Simulation,

Lp - Sound pressure level,

N - concentration of the polutant,

Re - Reynolds number,

St - Strouhal number,

t_1, t_2, t_3 – time steps,

v_∞ - velocity into free flow,

v_{ca} - velocity between cylinders into cascade.

INTRODUCTION

A previous study [1,2] of the axial fan guard grill on integral aerodynamic and sound characteristics determined the impact of the fan guard grill on the operation of the axial fan. The impact of the grill on the reduced efficiency of the fan and the increased emitted sound power level was studied in the case of an axial fan of 500 mm in diameter. A comparative study with the accompanying guard grill and without it was performed. It was determined that the guard grill causes a decrease in the operation ability; efficiency is reduced by 16% and noise generation is increased by 4 dB.

Based on the measured frequency spectrum of the sound power level, in case the fan operates with a guard grill, an increased sound power level in frequency spectra between 800 Hz and 2000 Hz, as illustrated by Figure 1, can be assumed. The elongated shape of the sound spectrum suggests an increased intensity of velocity fluctuations in the Karman street turbulent generation vortex structures. The phenomenon was presented in Alič et al. [1], analysed in the case of a cylinder cascade in a uniform air flow by various cascade angles and at various Re numbers. Velocity fluctuations were measured with a hot wire anemometer, a five-hole probe. The sound pressure level was also measured. Measurement results of the sound pressure level under the same conditions as the numerical model and experimental visualisation are illustrated in Figure 2.

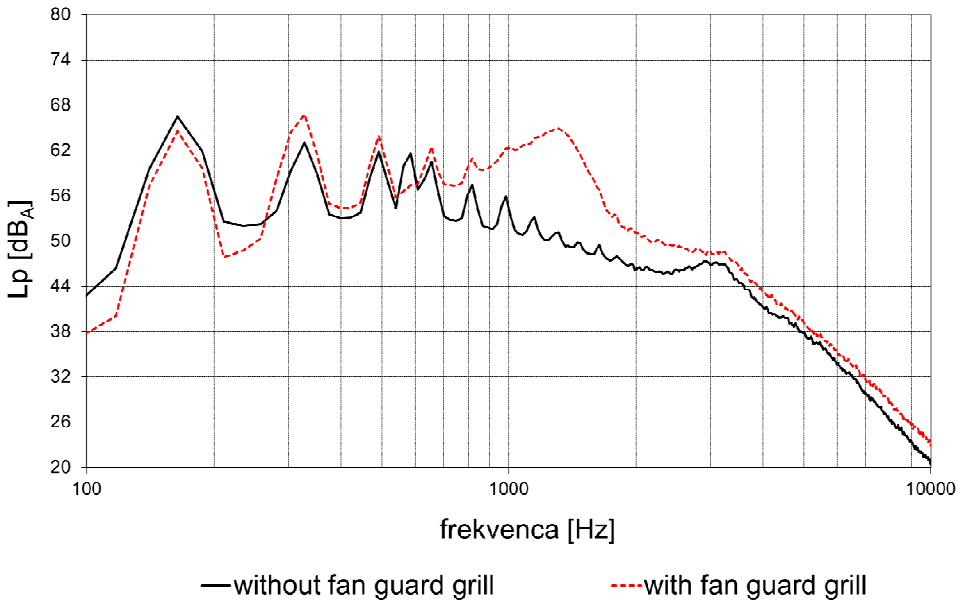

Figure 1: Measured fan sound pressure level with (red broken curve) and without the guard grill (black curve) [1].

Figure 2 shows significant differences between the generated background noise (Figure 2, red curve), noise on the isolated cylinder (Figure 2, blue curve) and the noise on the air flow around the cascade of cylinder (Figure 2, green curve). The emitted noise on the cylinder and the cascade is significantly greater than the background noise. The difference between the cylinder and the cascade is reflected in the increased sound pressure level and the atypical spectrum shape in the Karman vortex street range. The article seeks to present the aerodynamic and acoustic flow characteristics using experimental visualisations, measurements of the sound pressure level and a numerical simulation behind the cascade of cylinders (Figure 2, green curve). On the basis of measurements and a calculation, we seek to evaluate the presented variations in the spectra of the emitted sound power and the link between velocity fluctuations and the emitted sound power.

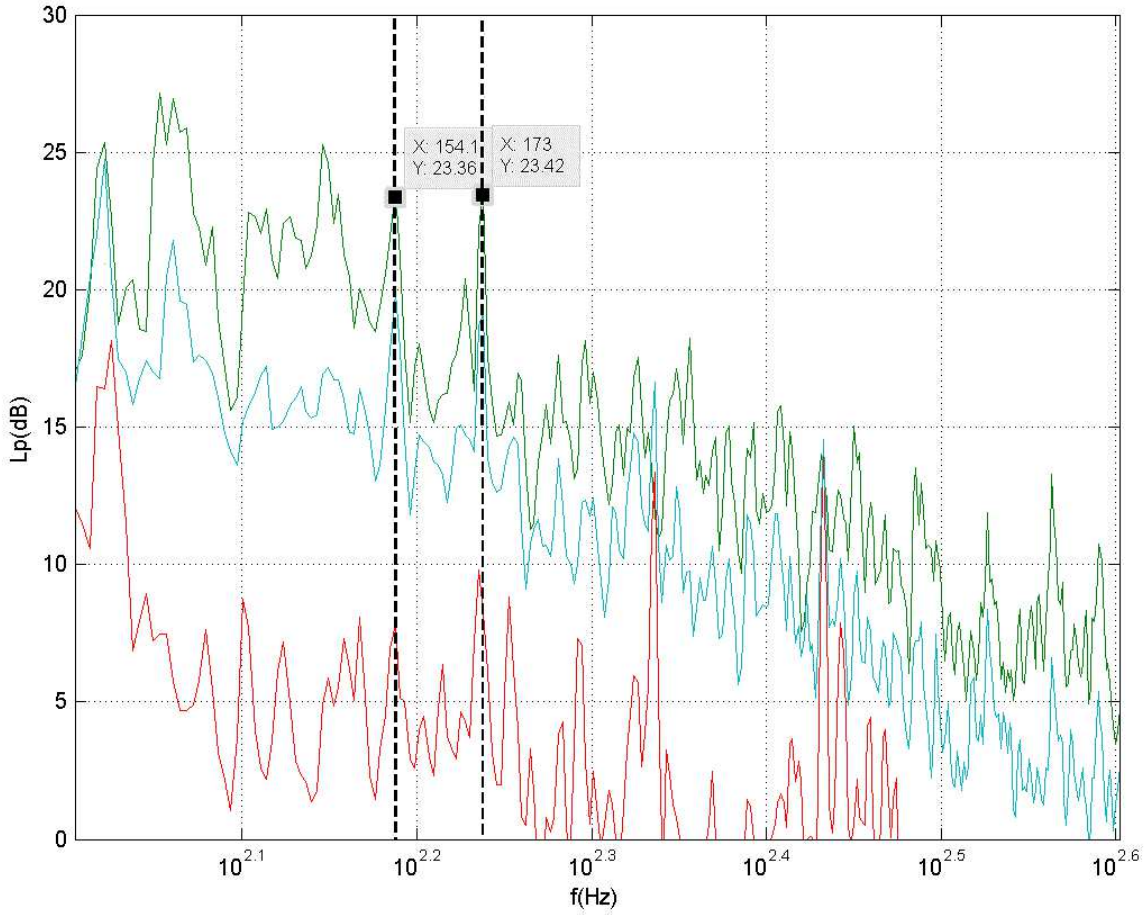

Figure 2: Sound pressure level in the far sound field for the cascade (green curve), cylinder (blue curve) and the background noise (red curve), Re = 3200 [1].

EXPERIMENTAL WORK

The experimental research was based on the flow field visualisation on a 5-cylinder cascade (Figure 3). For the purpose of the experimental work, the cylinders in the cascade are of a larger diameter (8 mm) than in the case of the axial fan guard grill (they were from 2,8 mm to 5 mm) [1]. By increasing the parameter of the bluff cylinder, the frequency of vortex generation behind the cylinder is reduced and facilitating the observation of vortex structures.

The vortices with frequency around 1400 Hz are very small and fast, therefore they are hard to detect and analyse with experimental visualisation. Because of these limits a larger diameter of test wire was selected. The larger wire diameter resulted in lower frequency of Karman street vortices. The Re number in case of airflow around wires of axial fan guard grill at fan optimal working point was in interval from 1500 to 4500. To achieve flow similarity between axial fan guard grill and cascade visualization experiment, we used the same Reynolds number interval in both experiments and Reynolds number for cascade experiment was set to 3200. We therefore selected inlet flow velocity for cascade experiment and numerical simulation such that the above Reynolds number was fulfilled.

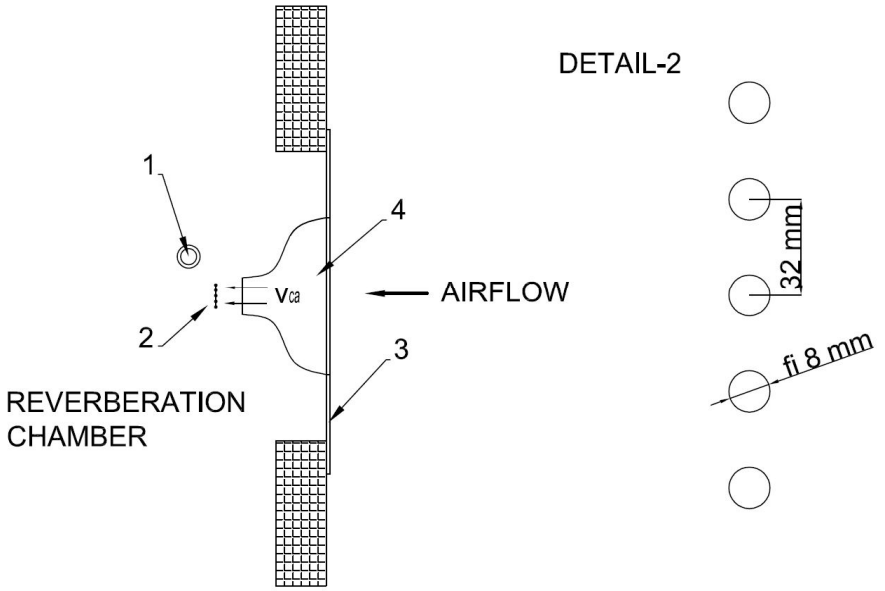

Figure 3: Left: Schematic experiment layout (1 – high-speed camera and microphone, 2 – cascade of cylinders, 3 – wall of the reverberation chamber, 4 – funnel), Right: detail of the cascade of cylinders.

The Karman structure generation frequency depends on the Strouhal number, on the velocity conditions and the diameter of the bluff cylinder. The distinct frequency of the cylinder bluffing vortex structure is given by equation 1 [3]:

Erreur ! Des objets ne peuvent pas être créés à partir des codes de champs de mise en forme. (1)

where *St* is the Strouhal number, *D* is the diameter of the cylinder, v_∞ is the velocity in the free flow field and *f* is the Karman vortex generation frequency. In the case of flow through the cascades of cylinders, those values are changed in view of the periodic placement of the cylinders, which reduces the free flow field. That is taken into consideration with a correction in equation 2:

Erreur ! Des objets ne peuvent pas être créés à partir des codes de champs de mise en forme. (2)

where velocity v_{ca} stands for the velocity conditions inside the cascade, characterised by the significantly increased local flow velocity. Hereinafter, the results are presented comparatively between experimental work by means of visualisation and the numerical model, in the operating point at a 90° cant angle of the cascade of cylinders (Figure 3) and Re 3200.

Experimental visualisation

The visualisation and all other previous integral, local measurements and measurements of the sound pressure level [1] were performed at the Hidria Institut Klima laboratory in Godovič. In view of the repeatability and comparability of various measurements, the placement and assembly of the cascade was the same as during the velocity measurements with the hot wire anemometer [1], during the measurements of the sound pressure level [4] and the visualisation of the vortex structures behind the cascade. The cascade visualisation scheme is illustrated in Figure 3.

The cascade was attached to the funnel (Figure 3, Point 4), which was attached to a board on the wall of the reverberation chamber (Figure 3, Point 3). The cascade was composed of five parallel

cylinders, placed in one plane (Figure 3, Point 2). The distance among the eight cylinders was four times the parameter of the cylinders (32 mm). The distance equalled the ratio between the spaces among the concentric guard wires and their parameter on the fans [1]. The length of the cylinders equalled two widths of the outlet orifice and on both sides joined by means of connecting cascade consoles that enabled the turn of the cascade. The ratio between the length of the cascade cylinders in the flow field and their diameter l_{cil}/D amounted to 12.5. Such a ratio is significantly higher than the recommended minimum ratio of 3.5 [5], whereby the permitted assumption of the vortex street generation is between the cylinder of finite length and the cylinder of the so-called infinite length.

Figure 4 illustrates a cylinder in the cascade (Figure 4, Point 1). The observed smoke pollutant (Figure 4, Point 2) is simulated on the shot by means of paraffin oil vapour on a resistance wire, heated by an electric current. The wire was placed inside the cylinder. The exit of the smoke pollutant into the air flow boundary layer was performed by means of drilled holes of 1 mm in diameter (Figure 4, Position A). The 5×5 pixel small squares (Figure 4, Point 3) mark the measuring points where later on, during the digital shot sequence processing procedure, grey levels were analysed. Fifteen windows of 1D (D = diameter of the cylinder) mutual distance were selected.

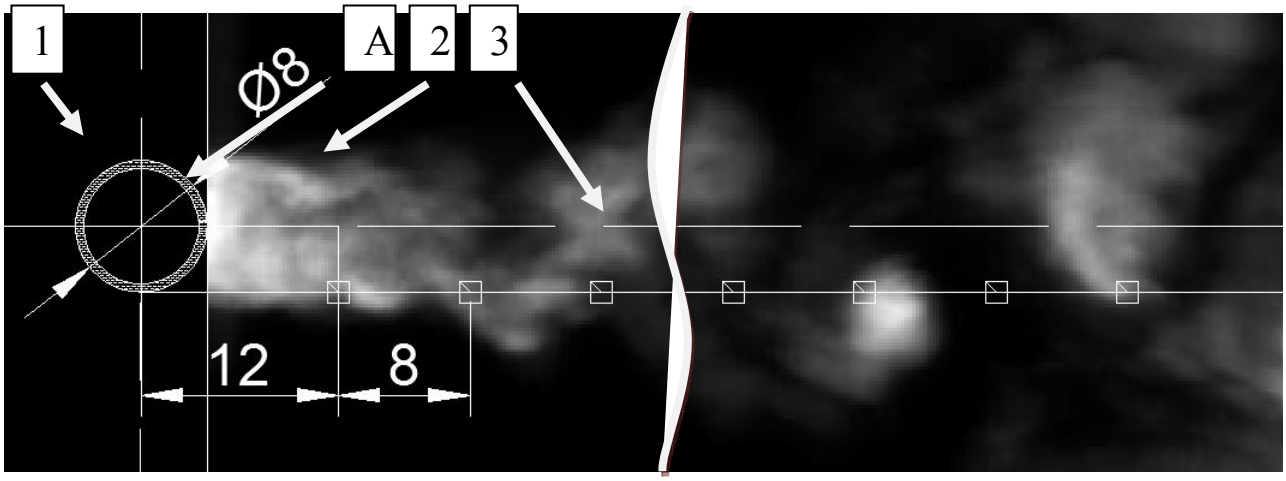

Figure 4: The bluff cylinder inside the cascade. The squares mark the signal collection points.

It was assumed that the values of the scalar grey level field would be proportional to the proportion of the pollutant in the observed window and that the pollutant or grey level concentration fluctuations would be proportional to the velocity fluctuations [6]:

Erreur ! Des objets ne peuvent pas être créés à partir des codes de champs de mise en forme. (3)

Symbol A stands for the observed variable of the grey level intensity in the active window, N for the concentration of the pollutant in the observed area. The A variable is of a whole number value in the range between 0 and 255, which changes with time for the given window, determined by the coordinates (x, y). The relation between the grey level and the pollutant proportion is given by:

Erreur ! Des objets ne peuvent pas être créés à partir des codes de champs de mise en forme. (4)

whereby $E(i, j)$ is the whole number value of the pixel grey level in the active window [7]. The significant time series for the case of the operating point at Re 3200 for the measuring point in window 5 (Figure 4, fifth window from right to left) is presented in Figure 5. By means of FFT

algorithms, the signals were then transformed into a frequency area, which shows the value of the grey level depending on the frequency. The collection of digital shots (Figure 3, Point 1) was performed with a 2.4 kHz frequency, which enables the analysis of the frequency spectrum up to the 1.2 kHz frequency range. The camera used for image acquisition was B&W camera FASTEC HISPEC 4 with high sensitivity CMOS sensor. Camera operated at resolution 864x620 pixels, 2400 Hz frame rate and exposure time 350 µs. Nikkor 50 mm/F1.2. megapixel lens was used. Aperture of the lenses was F4. Vortices were illuminated using eight CREE XM-L T6 LED lights, four from above and four from below. Light sheet was generated using 70 mm cylinder lenses, mounted on LED lights. Power for the LED lights was provided by continuous DC power supply, resulting in a flicker free illumination. Image processing and signal collection was performed by means of the Dynascan computer software; frequency spectra were calculated in the Matlab environment.

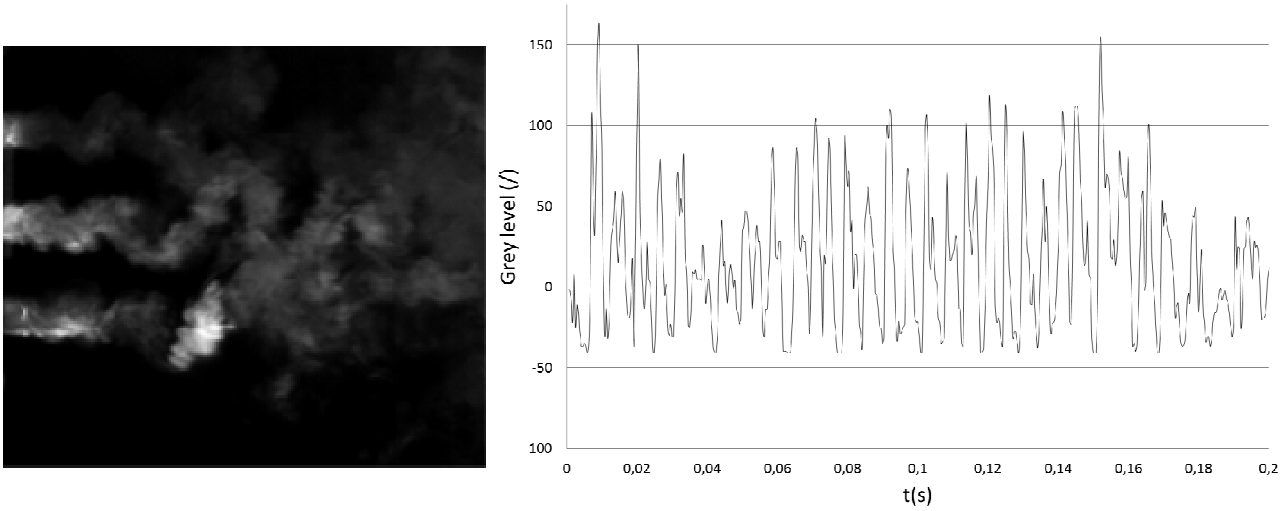

Figure 5: The figure on the left represents the smoke pollutant for the cascade of cylinders; the figure on the right the signal of the grey level depending on the time step.

The presented smoke pollutant bluffing behind the cascade provides information on the fluctuation of the grey level scalar field. Because the observed phenomenon is spatial, certain limitations in the application of the visualisation method apply. These limitations hinder the analysis of the vortex structures. The visualisation also does not provide information on the pressure and velocity field. Therefore, a numerical simulation was performed, which is presented below.

NUMERICAL SIMULATION

The study of the vortex structure interaction involved a numerical simulation with LES – Smagorinsky [8], by means of which results on the velocity field fluctuation, the sound pressure level [9], [10] and a detailed analysis of the discussed work that is presented in this article have been obtained. The LES numerical model was chosen in view of observing the non-stationary decay of the vortex structure and their mutual interactions. The calculation was done in the ANSYS CFX programme package.

Two grids densities with (i) 2.3×10^6 and (ii) 5.07×10^6 elements and three different time steps were tested. It was determined that the chosen grid densities and shapes do not impact the result of the frequency fluctuation distribution calculation, thus eliminating the impact of the grid on the calculation result. With the purpose of selecting sufficiently small time steps, the following time steps were chosen: $t_1 = 0.001$ s, $t_2 = 0.005$ s and $t_3 = 0.00025$ s were chosen. The time step t_1 proved unsuitable, while the difference between t_2 and t_3 was considered negligible. Figure 6 shows the

numerical model of cascade and contours of the same velocity. The white and yellow cross-sections along the plane mark represent the observed points of velocity fluctuation and sound pressure level. Same points are also shown in Figs. 8-11. The simulation was done for Re =3200, which was the same condition as in case of experimental visualisation.

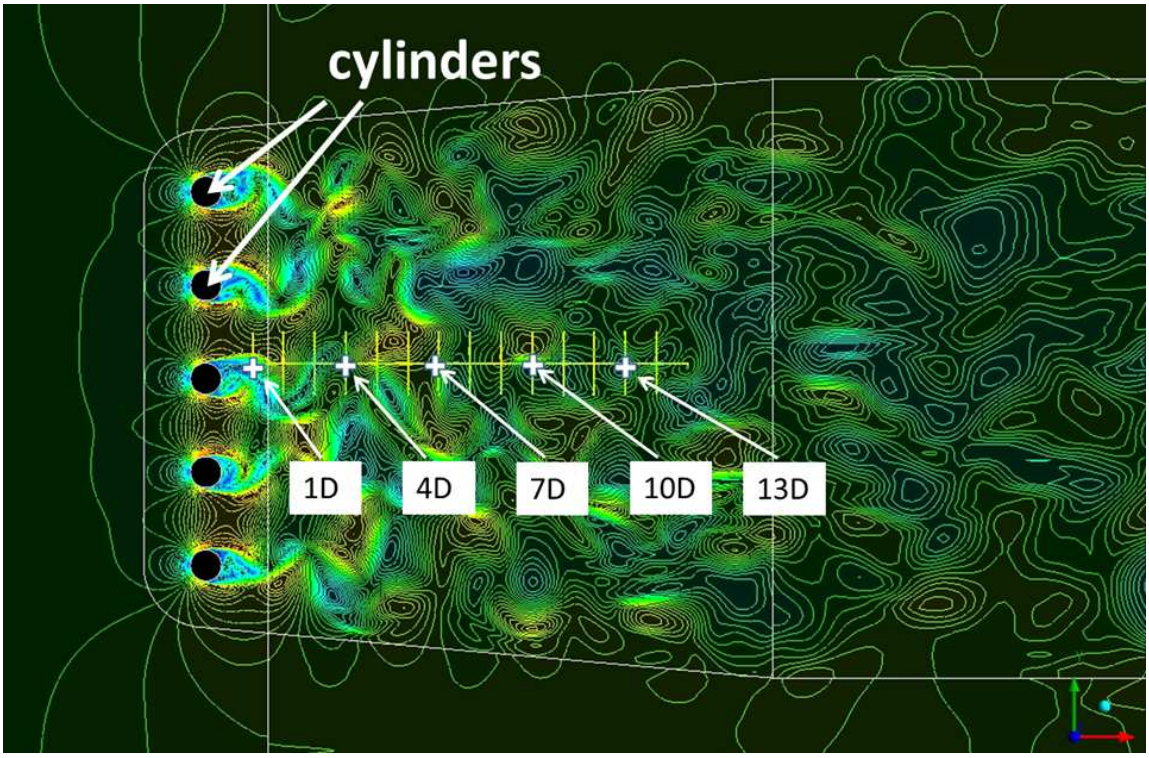

Figure 6: Numerical model with contour of the same velocity and positions of observing points (from 1D to 14D).

COMPARISON BETWEEN THE EXPERIMENTAL AND THE NUMERICAL PART OF THE RESEARCH

Comparison between numerical simulation and experimental visualisation at the same conditions are shown in figure 7. On left part of the figure 7, a LES simulation of velocity distribution is shown. Velocity is represented by a grey scale. On right part of the figure 7, a picture of experimental visualisation with polutant is shown. Although left and right of figure 7 represents different variables, velocity and concentration, similarity of patterns may be observed.

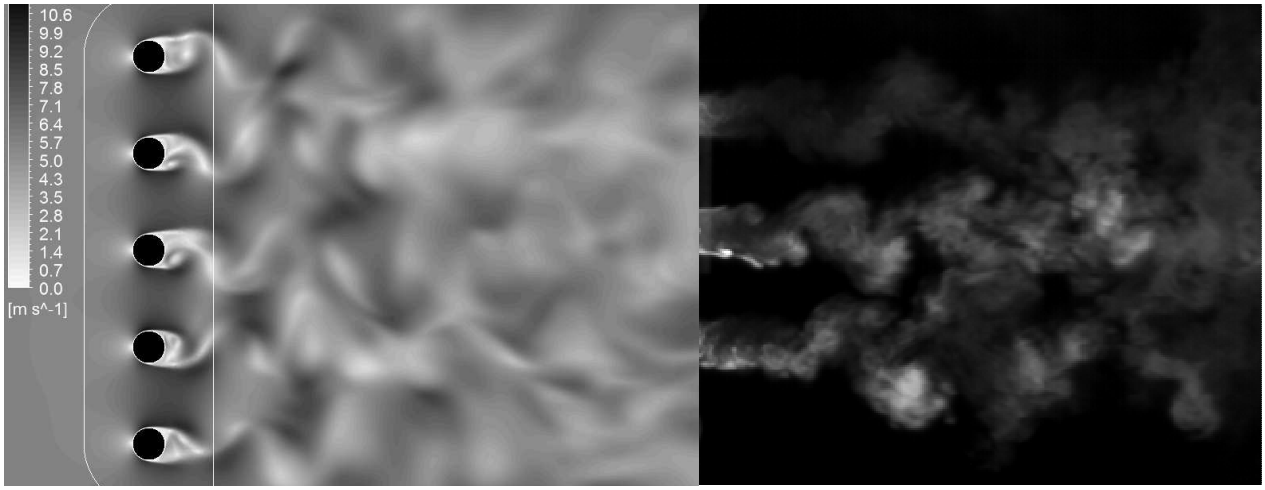

Figure 7: Numerical model (left: velocity), experimental visualization (right, concentration).

The results of the experimental work by means of visualisation were analysed at various distances from the cylinders inside the cascade in the air flow direction. Figure 8 illustrates the grey level depending on the grey level changing frequency and the distance from the median rod of the cascade. In Figure 8, two more pronounced peaks in the 170 Hz and 340 Hz frequency range can be observed. The first peak stands for Karman frequency, the other reef corresponds to the first harmonic of the Karman vortex street frequency. The generation of peaks and their progressive lowering can be observed in the over 170 Hz frequency range.

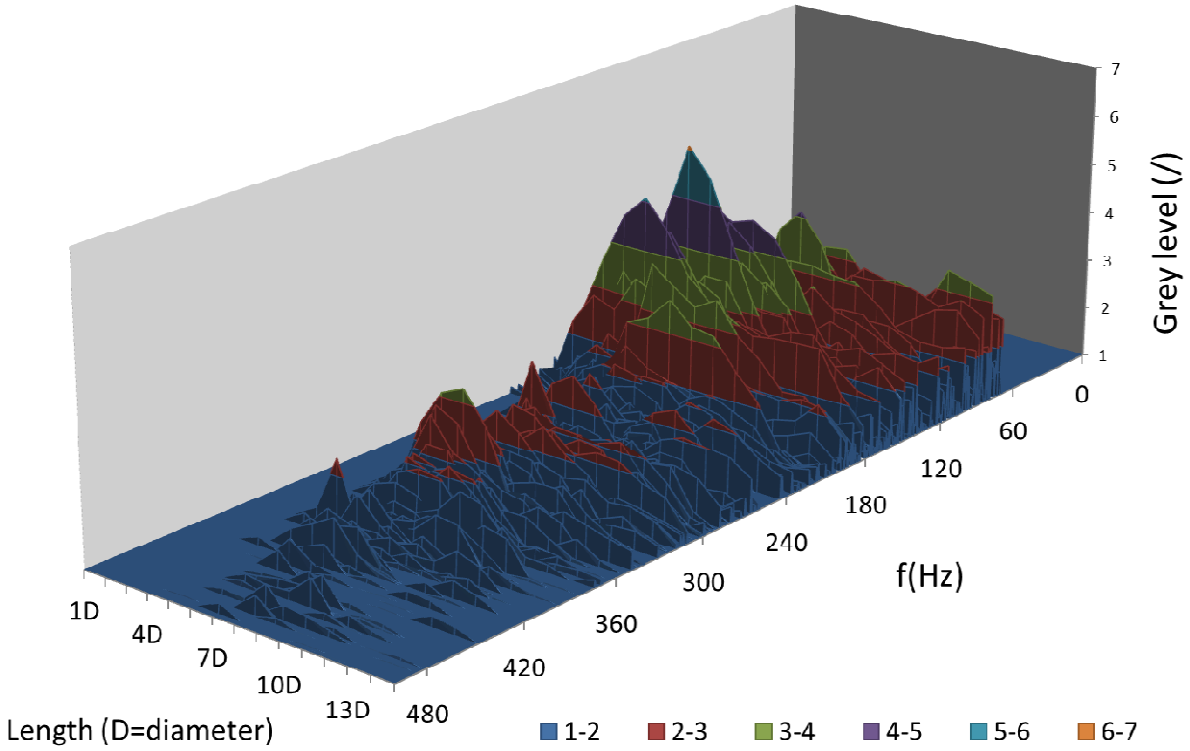

Figure 8: Visualisation grey level depending on the frequency and distance from the cascade.

The frequency back generation range decreases in the form of a wedge by increasing the frequency. What has been observed can be attributed to the vortex structure decay and the interaction among

them. The spectrum shape in the higher frequency range is also subject to diffusion mechanisms, which follow the vortex decay.

Figure 9 illustrates the amplitude of the numerically modelled velocity depending on the fluctuation frequency and the distance from the median rod of the cascade. At the same operating point, where the experimental work case was discussed, in Figure 9, two increased peaks in the 170 Hz and 340 Hz frequency range can be observed. The frequency peak minimally differs from the calculated frequency according to equation 2. The frequency peaks of the velocity field oscillation and the pollutant's scalar field are minimally shifted. The generated difference remains within measurement uncertainty.

A significantly increased reef, which corresponds to the Karman vortex street, can be observed. The velocity amplitude at 170 Hz increases from a minimum value at a distance of 1D to the maximum value at 15D of the observed fall length.

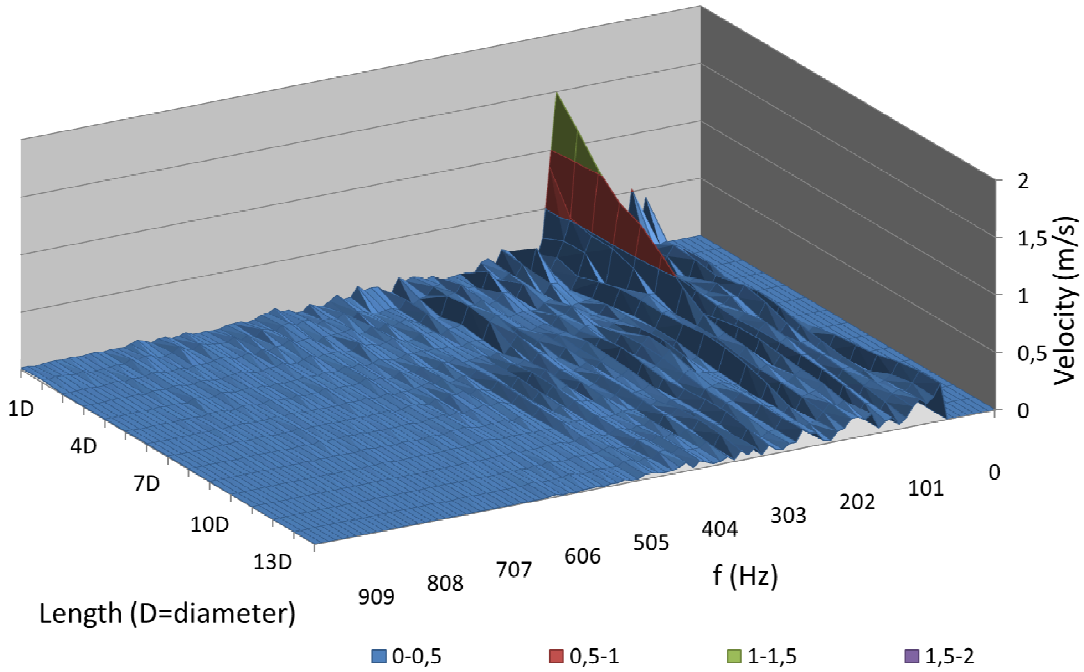

Figure 9: Velocity fluctuation amplitude depending on the frequency and the distance from the cascade.

Figure 10 illustrates grey level depending on the frequency axis (Figure 10, blue curve) and the numerically calculated velocity fluctuation for the time step t_3 at the chosen distance 5D. The graph also illustrates the difference between the numerically calculated frequency spectra for the case of 1 cylinder (Figure 10, green curve) and of a cascade of cylinders (Figure 10, red curve). The numerically calculated frequency peak A = 151 Hz for the cylinder case matches the theoretical calculation according to equation 1.

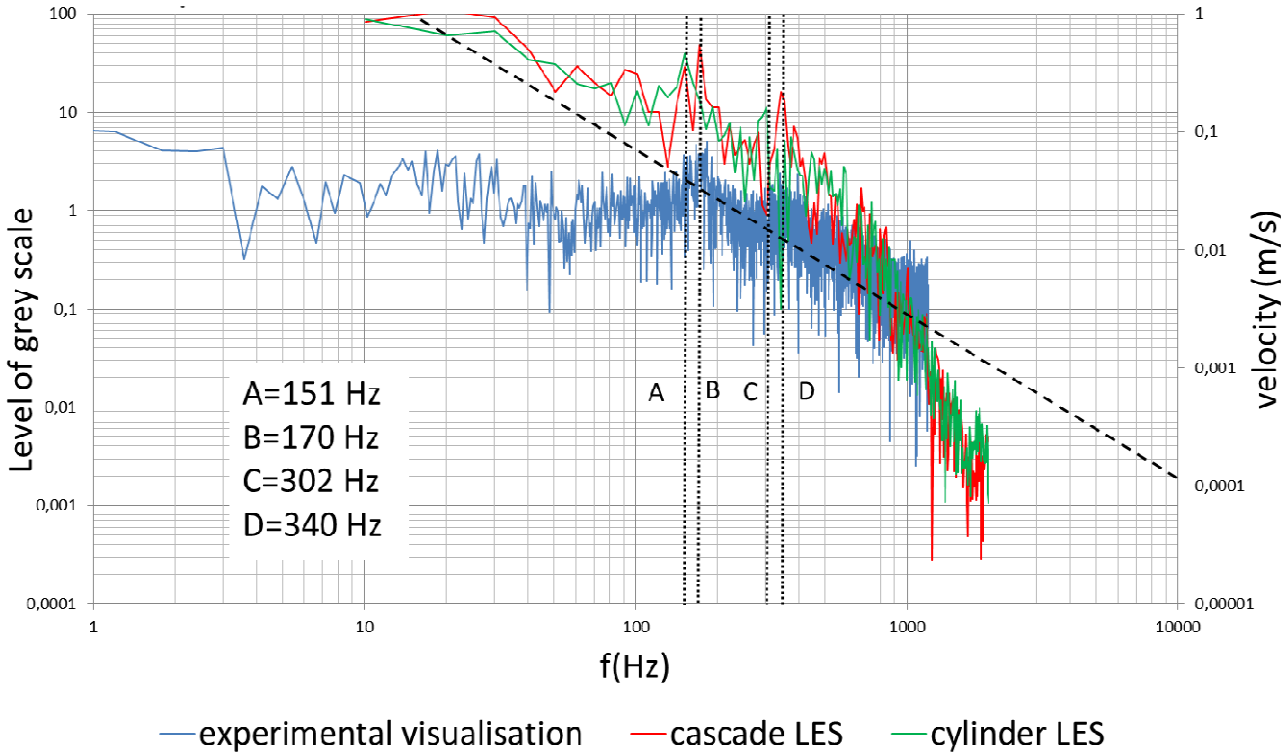

Figure 10: Grey level and velocity fluctuation depending on the frequency axis at a distance of 5D.

Along with the increased grey level for the cascade case at A = 151 Hz, B = 170 Hz and D = 340 Hz, the characteristics of *-5/3* cascade decay of a fully developed isotropic turbulence (Figure 10, italic broken line) can be observed. Pursuant to the expected, it can be observed that the modelled values are adjusted to the *-5/3* dissipation law of fully developed isotropic turbulence. In the higher frequency area, the calculated dissipation of energy is excessive, which is also shown on the diagram in Figure 10. Excessive vortex structure decay is a result of a too low grill density and of a too short calculation step for the higher frequency range. Figure 11 illustrates a modelled emitted sound pressure level for 1 cylinder (Figure 11, blue curve) and for the cascade (Figure 11, red curve). The difference between the modelled sound pressure level in the near field and the measured sound pressure level in the far field (Figure 2) differs in amplitude and partially also in the shape of the frequency spectrum. The difference is a result of non-observation of the back ground noise generation in numerical case and the interaction between the jet noise and stationary air, which enters a large space through the cascade. Basic Karman vortex shedding frequencies can be observed by both spectra.

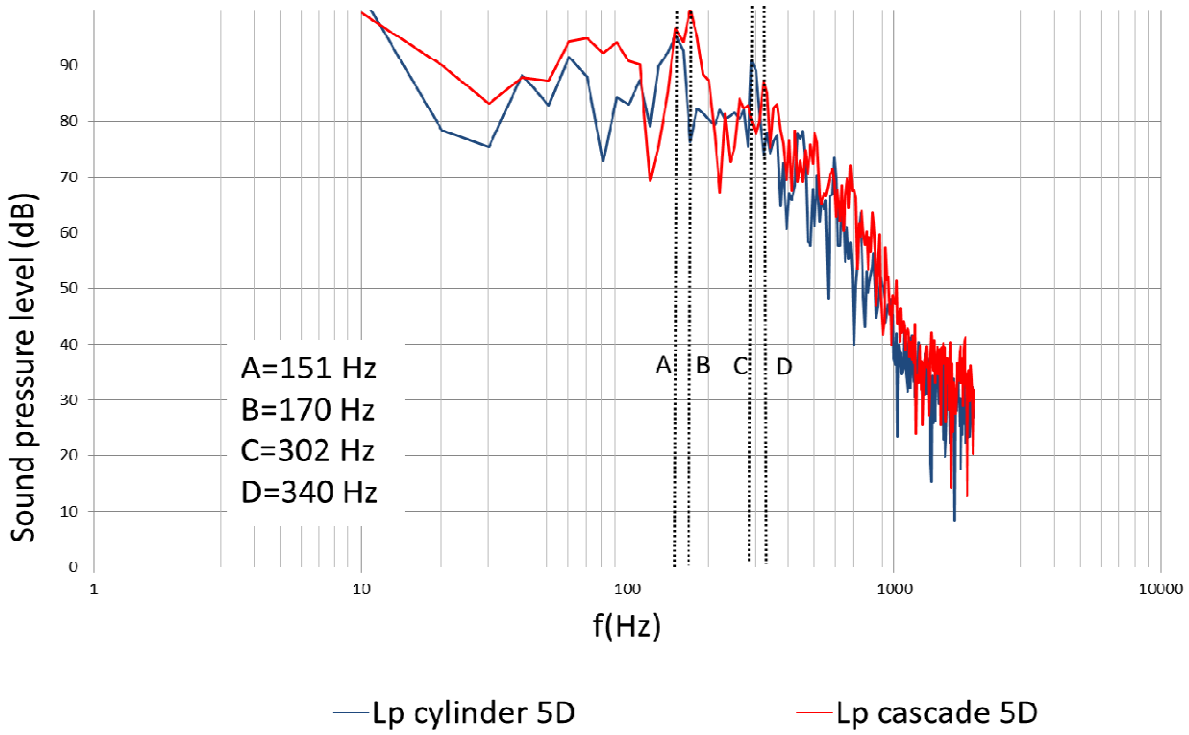

Figure 11: Numerical calculation of sound pressure level in near field at a distance 5D from the cascade.

CONCLUSION

This vortex generation study behind the cascade of cylinders that simulated a segment of the axial fan guard grill included an experimental visualisation with a smoke pollutant and sound pressure measurement results in the far sound field. In the example of the cascade of cylinders, a numerical calculation of the velocity fluctuations and the sound pressure level in the near sound field for the case of an isolated cylinder and a cascade of cylinders was also done. The objective of the study was two-fold. Based on already known physical facts on Karman vortex generation and -5/3 cascade decay of a fully developed isotropic turbulence behind a cylinder, it attempted to review the adequacy of the experimental methods and the numerical models for the purpose of researching aero-acoustic phenomena in the axial fan area and its surroundings. The second objective of the research was to confirm the assumption from the study [1] that the source of increased sound pressure in the far sound field for the cascade of cylinders case and consequently also for the axial fan grill could cause Karman vortex generation. Additional numerical noise calculations of Karman vortex generation in the near sound field, which more markedly confirm the origin of noise in the air flow, serve as complementary measurements of sound pressure level measurements in the far sound field in Figure 2 [1], which inconspicuously suggest that Karman vortex generation can be perceived. Reason of slightly marked frequency peak in cascade case of far field sound pressure level measurements is in low intensity of velocity fluctuations. It is known by Proudman acoustic model [11] that emitted sound pressure of high Reynolds number isotropic turbulence is in correlation with fifth power of velocity fluctuation.

In case of operation of the axial fan, it could be concluded that in view of the non-homogeneous velocity conditions on the guard grill, vortex generation takes place with greater intensity, which results in a greater and more marked generation of noise in larger frequency region, as illustrated in Figure 1 [1].

The fan grill design must ensure sufficient structural strength and protection from interference with upper limbs to the fan rotor during operation. In addition to the above requirements, we have shown that fan grill contributes to unwanted noise generation and for further designs we want to reduce noise generation to the minimum. As prototyping of new grills and their measurements are expensive and time consuming, we have proposed a LES flow modelling method, which may reduce requirements for grill prototyping and measurements. The LES flow modelling method proved satisfactory in modelling flow fluctuations and noise generation on fan grills, therefore the method may be used for future fan grill designs.

REFERENCES

[1] G. Alič, B. Širok, M. Hočevar - *Method for modifying axial fan's guard grill and its impact on operating characteristic.* Forsch. Ing. wes., vol. 74, pp. 2, str. 87-98, Jun. **2010**,

[2]. G. Alič, B. Širok, M. Hočevar - *Guard grill impact on aerodynamic integral and acoustic characteristics of an axial fan.* Noise Control Eng. J., vol. 58, iss. 3, pp. 223-242, **2010,**

[3] F. White – Fluid *Mechanics* – 4th ed., McGraw Hill, **1999,**

[4] M. Milavec, B. Širok, M. Hočevar, M. Eberlinc - *Mechanism of vortex generation behind the cylinder cascade*, Kuhljevi dnevi, vol 2, pp. 145-152, **2011**,

[5] J. M. R. Graham – *The effect of end plates on the two-dimensionality of vortex wake*, Aero, **1969,**

[6] M. Novak, M. Hočevar, B. Širok, D. Philpott, David R., Bullen, Peter R. - *Analysis of turbulent mixing flow of a bluff body wake using a computer vision system.* J. flow vis. image process, vol. 6, no. 3, pp. 231-242, **1999,**

[7] M. Novak, M. Hočevar, B. Širok, M. Oberdank Kazimir - *Simultaneous measurement of velocity fluctuations and smoke tracer fluctuations of turbulent flow over a back-facing step*. J. flow vis. image process, vol. 6, no. 3, str. 221-229, **1999,**

[8] ANSYS CFX – *Release 12.0, ANSYS CFX – Solver Theory Guide*, **2009.**

[9] R. Meier - Staude, M. Kuntz – *Wind turbine modeling using ANSYS*, ANSYS Inc., **2006.**

[10] D. Robinson – *Acoustic modeling in CFX*. The focus, A publication for ANSYS users, November **2007,**

[11] R. Rubinstein, Y. Zhou – *Sweeping and straining effects in sound generation by high reynods number isotropic turbulence*, National Aeronautics and Space Administration under NASA Contract No. NAS1-19480,